https://doi.org/10.5194/egusphere-2026-3087
Preprint. Discussion started: 2 July 2026

Revealing the Mechanistic Linkage Between QBO-Modulated Stratospheric Dynamics and Southern Tibetan Plateau Precipitation by Stratospheric $^{10}Be/^{7}Be$ Isotope Characteristics

Xuke Liu[1,3#], Nanjian Liu[5,6,#], Yunchong Fu[1,3,4*], Guocheng Dong[1,3], Li Zhang[1,3], Xinyi Du[1,6], Yanting Bi[2]

1. State Key Laboratory of Loess Science, Institute of Earth Environment, Chinese Academy of Sciences, Xi'an, 710061, China

2. Xi'an Institute for Innovative Earth Environment Research, Xi'an, 710061, China

3. Shaanxi Key Laboratory of Accelerator Mass Spectrometry Technology and Application, Xi'an AMS Center of IEECAS, Xi'an 710061, China

4. Institute of Global Environmental Change, Xi'an Jiaotong University, Xi'an, 710049, China

5. Institute of Geographic Sciences and Natural Resources Research, Chinese Academy of Sciences, Beijing, 100101, China

6. University of Chinese Academy of Sciences, Beijing, 100049, China

#The authors contribution equally to this work and should be considered co-first authors

**Corresponding author: Yunchong Fu, E-mail: fuyc@ieecas.cn*

Abstract: The Tibetan Plateau, a pivotal component of the global climate system known as the "Asian Water Tower," governs freshwater availability for billions. However, the physical mechanisms linking stratospheric circulation to its precipitation variability remain poorly constrained, limiting predictive understanding. Here, this work constructs a new indicator based on the ratio of stratospheric tracer ^{10}Be ($t_{1/2}$ = 1.39 Ma) and ^{7}Be ($t_{1/2}$ = 53.29 d), to reveal the modulation mechanism of stratospheric Quasi-Biennial Oscillation (QBO) phase transitions on Tibetan Plateau precipitation processes and its possible large-scale vertical circulation associations. Analyzing synchronous wet-deposition data from Lhasa (Tibetan Plateau) and Xi'an (Loess Plateau) during the 2022–2023 QBO transition, we empirically analyzes the synchronous response relationship between isotope deposition and regional precipitation during the tropopause stable

https://doi.org/10.5194/egusphere-2026-3087
Preprint. Discussion started: 2 July 2026

period determined by the $^{10}Be/^{7}Be$ ratio in precipitation samples. An XGBoost machine-learning model then isolates the coupled impact of the easterly QBO phase and upper-level circulation on precipitation. Our results demonstrate that during the observation period, the easterly QBO excites a meridional wind dipole, driving an anticyclonic circulation that enhances stratospheric air transport to the surface. This dynamical pathway substantially increases precipitation in the southern Tibetan Plateau by approximately 31%. Attempting to mechanistically linking a fundamental mode of global atmospheric variability to regional water resources via stratospheric isotopic evidence, this framework advances the understanding of cross-scale interactions within the Earth system, with direct implications for evaluating climate model performance and future water security under global change.

Keywords: Quasi-biennial oscillation, Stratospheric tracer, East Asian monsoon, Precipitation, Machine learning

1. Introduction

The Tibetan Plateau, known as the "Asian Water Tower," has precipitation changes that profoundly affect the Asian monsoon system and regional water resource security (Yang et al., 2014). Against the backdrop of global climate change, increased monsoon variability has led to enhanced interannual fluctuations in precipitation across the plateau and downstream regions, resulting in frequent extreme hydrological events that seriously threaten regional ecological security and socioeconomic stability (Willner et al., 2018; IPCC, 2021). Over the past 20 years, meteorological disasters have caused China to lose approximately 370 billion yuan annually and

https://doi.org/10.5194/egusphere-2026-3087
Preprint. Discussion started: 2 July 2026

led to the deaths of about 1700 people (Li et al., 2021). Over the next 20 years, changes in precipitation that trigger river floods will increase China's total economic losses by 82% (Willner et al., 2018). Therefore, clarifying the driving mechanisms of precipitation on the Tibetan Plateau is an urgent need for understanding monsoon evolution, improving climate prediction, and developing adaptation strategies.

Against this backdrop, the evolutionary trends of atmospheric vertical structure (including tropopause height, stratosphere-troposphere exchange intensity, etc.) and their hydroclimatic effects have become a cutting-edge research topic in the study of rainfall driving mechanisms in High Asia. Among these, the stratospheric Quasi-Biennial Oscillation (QBO), as an important stratospheric dynamic process, has been confirmed to be a key factor leading to the north-south dipole mode of precipitation in East Asia centered around 30°N, typically expressed as either "southern drought-northern flood" or the reverse (Hu et al., 2022; Zhang et al., 2024; Fu et al., 2024). The QBO refers to the periodic alternation of easterly and westerly zonal winds in the tropical stratosphere, with easterly (EQBO) and westerly (WQBO) phases alternating approximately every 28 months (Ebdon and Veryard, 1961). The QBO signal propagates downwards from 30 hPa to the lower stratosphere and has a strong regulatory effect on stratospheric and tropospheric circulation (Baldwin & Dunkerton, 1991; Hitchman et al., 2021). The QBO can influence the intensity and structure of the stratospheric polar vortex, alter subtropical jet stream dynamics, and regulate deep convective activity in monsoon regions (Collimore et al., 2003). In East Asia, these atmospheric circulation changes caused by the QBO fundamentally affect the spatiotemporal distribution of monsoon rainfall (Zhang et al., 2023; Luo et al., 2023; Zhang et al., 2024). Previous studies have shown that the impact of the QBO on the

https://doi.org/10.5194/egusphere-2026-3087
Preprint. Discussion started: 2 July 2026

surface is mainly concentrated in winter, but it is gradually being recognized that the QBO may also have a significant impact on summer rainfall (Ho et al., 2009; Hu et al., 2022). For example, during the EQBO phase, enhanced convective transport and moisture flux can strengthen precipitation in key regions such as the Tibetan Plateau, while the WQBO period usually suppresses these processes (Hu et al., 2022). However, there is currently a lack of sufficient direct observational evidence regarding the specific mechanisms by which the QBO influences summer precipitation over the Tibetan Plateau through stratosphere-troposphere coupling, particularly high-resolution indicators that can effectively trace atmospheric vertical exchange processes.

Traditional methods for identifying precipitation driving factors in high-altitude regions largely rely on meteorological reanalysis data or climate model simulations. Although China has gradually increased upper-air observations in the Tibetan Plateau during recent years (MA et al., 2023), it remains difficult to achieve regional long-term continuous monitoring, and there is a lack of high-resolution physical tracer information in the vertical direction. Collecting isotopic indicators from surface samples has become a continuous observation method, capable of effectively responding to rainfall events and processes (Yu et al., 2025; Chen et al., 2020; Heikkilä and Smith, 2013). Cosmogenic isotopes are a special type of isotopes that are naturally produced solely through cosmic ray interactions. Early studies utilized cosmogenic beryllium-7 (^{7}Be) and beryllium-10 (^{10}Be) as passive tracers to reveal stratospheric anomalies (Raisbeck et al., 1981; Zanis et al., 2003). ^{7}Be and ^{10}Be are produced by the interaction of cosmic rays with N and O atoms in the stratosphere and tropopause (Masarik and Beer 1999). Once generated, ^{7}Be and ^{10}Be quickly adsorb onto submicron aerosols and participate in the entire atmospheric mixing process (Graham et al., 2003). The distinct production locations and half-lives of ^{7}Be (half-life: 53.29 days)

https://doi.org/10.5194/egusphere-2026-3087
Preprint. Discussion started: 2 July 2026

and ^{10}Be (half-life: 1.39 million years) allow us to distinguish air masses originating from the stratosphere and troposphere (Yamagata et al., 2010), while their deposition fluxes provide insights into moisture scavenging processes (Graham et al., 2003; Heikkilä and Smith, 2013). In particular, the ^{10}Be/^{7}Be ratio has been widely used as a sensitive indicator of stratosphere-troposphere transport (Liu et al., 2022; Liu et al., 2024a), with the potential to capture the downward transport of air masses caused by stratospheric dynamic processes such as the QBO and their impact on surface precipitation dynamics. Therefore, these cosmogenic radionuclides are expected to become a key bridge connecting large-scale circulation changes with regional hydrological responses, providing a novel and powerful research tool for a deeper understanding of the formation mechanisms and variability patterns of monsoon precipitation.

This work aims to provide new methods and direct evidence for revealing the mechanisms by which stratospheric dynamic processes influence the surface hydrology and climate of the Tibetan Plateau through long-term field observations of cosmogenic ^{7}Be and ^{10}Be in precipitation. The Tibetan Plateau, influenced by the deep convective activity of the Asian monsoon and its high-altitude topography, is extremely sensitive to changes in stratosphere-troposphere material exchange and water vapor transport (Bian et al., 2020). By analyzing the temporal variations of ^{7}Be and ^{10}Be wet deposition fluxes in Lhasa (3650 m a.s.l.) on the Tibetan Plateau, linking them to Asian regional atmospheric circulation dynamics, and simultaneously comparing them with Xi'an (420 m a.s.l.) on the Loess Plateau, which is affected by similar large-scale circulation, and combining machine learning methods, we focus on analyzing the stratospheric-tropospheric coupling process modulated by the QBO and separating its key driving role in precipitation variability. This work will provide new in-situ observational evidence and an interdisciplinary

https://doi.org/10.5194/egusphere-2026-3087
Preprint. Discussion started: 2 July 2026

research perspective for understanding how large-scale circulation changes in East Asia drive regional precipitation responses.

2. Materials and methods

2.1 Study area

The Tibetan Plateau averages over 4000 meters in elevation and is characterized by limited precipitation, low pressure, and intense solar radiation. The region's natural setting is highly complex and distinctive, especially regarding precipitation patterns. Precipitation across the Tibetan Plateau is generally low, with most rainfall occurring in summer, especially during July and August. Under the combined effects of the East Asian and Indian monsoons, rainfall is unevenly distributed (higher in the eastern and southern regions), and lower in the western and northern areas. The plateau's precipitation is primarily shaped by its terrain, monsoon systems, and atmospheric circulation, influencing both regional ecosystems and the climate in adjacent areas. The sampling location, Lhasa, lies in the southern Tibetan Plateau, receiving roughly 400 mm of annual rainfall and sitting at an average altitude of 3600 m.

The Loess Plateau is adjacent to the Tibetan Plateau and is influenced by the same large-scale atmospheric circulation patterns. Furthermore, it is located on the same side of the dipole rainfall pattern as the Tibetan Plateau, and is therefore used as a control observation point in this work. Rainfall also exerts a significant impact on the vulnerable ecosystems of the Loess Plateau: too much can intensify soil erosion and geomorphic degradation, while too little may lead to reduced vegetation cover and weakened ecosystem functions (Cai et al., 2022). According to Chinese Loess ^{10}Be sedimentary records, climate change has historically caused variations in the intensity

https://doi.org/10.5194/egusphere-2026-3087
Preprint. Discussion started: 2 July 2026

of rainfall events on the Loess Plateau (Zhou et al., 2023). Xi'an, where sampling was conducted, lies in the southern Loess Plateau of China and receives approximately 500-750 mm of rainfall annually.

2.2 Sample collection

In the rainy seasons of 2022–2023 (Mar.to Sep.), we obtained 60 precipitation samples from Lhasa, located in the southern Tibetan Plateau [29°38′49″N, 91°4′37″E, 3650 m above sea level (a.s.l.)], and Xi'an in the southern Loess Plateau (34°13′20″N, 109°00′18″E, 420 m a.s.l.). Outside of this period, either there was almost no rainfall or the precipitation volume was insufficient for effective sample collection. The Lhasa site is encircled by mountain ranges, whereas the Xi'an site lies in the Guanzhong Basin, north of the Qinling Mountains (geographical setting shown in Fig. S1). Samples were collected from rooftop locations at both sites (~18 m above ground in Lhasa and ~5 m in Xi'an). The volume of each sample ranged is 4-120 L, with the duration of collection determined by rainfall amount, not exceeding 24 h. Rainwater was collected over areas of 4·0.28 m^2 in Lhasa and 6·0.28 m^2 in Xi'an. Rainwater was collected and stored using acid-cleaned polyethylene trays and polyethylene containers. The acid pre-treatment of containers minimizes adsorption of ^{7}Be and ^{10}Be on container surfaces (Tiessen et al., 2019). The first ~0.5 hours of rainfall were excluded to eliminate contamination from re-suspended ^{10}Be in dust, allowing for reliable measurements of wet ^{10}Be deposition (Graham et al., 2003). The sampling times provided in this work are local time (UTC+8).

2.3 Laboratory analysis

Unlike the conventional need for gamma spectrometry to measure short half-life of ^{7}Be, we applied accelerator mass spectrometry (AMS) to simultaneously analyze both ^{7}Be and ^{10}Be. Both

https://doi.org/10.5194/egusphere-2026-3087
Preprint. Discussion started: 2 July 2026

$^{7}Be/^{9}Be$ and $^{10}Be/^{9}Be$ were measured on the same AMS targets prepared with a known quantity of stable ^{9}Be, streamlining the $^{10}Be/^{7}Be$ data acquisition. Each sample was processed in 10-20 min, allowing for efficient collection of large volumes of high-precision beryllium isotope data. The chemical pretreatment aimed to extract and purify beryllium from the samples, and ultimately produce BeO solid targets for AMS analysis (Fig. S2). The experimental procedures for sample pretreatment and AMS target preparation were based on previously published methods for rainwater processing (Zhang and Fu, 2017), with a minimum acceptable recovery rate of > 80%. The ^{9}Be standard solution (1000 mg/L) from NCS Testing Technology Co. Ltd and the ^{10}Be standard (SRM 4325, $^{10}Be/^{9}Be = 2.68 \cdot 10^{-11}$) from National Institute of Standards and Technology were applied in the analysis. Dowex1W-X8 (Cl^-) ion exchange resin (Merck) was employed in conjunction with a Bio-Rad ion exchange column (1.0 cm×20 cm). Additional reagents comprised analytical-grade HNO_3, HCl, $NH_3 \cdot H_2O$, H_2O_2, along with Milli-Q purified H_2O (resistivity = 18.2 MΩ·cm, 25 °C).

2.4 AMS measurement sample

^{7}Be and ^{10}Be analyses were carried out at the Xi'an Accelerator Mass Spectrometry Center by 3MV multi-isotope AMS system. Both ^{7}Be and ^{10}Be were measured concurrently on a single target in a +4 charge state, with analytical conditions based on previously published parameters (Liu et al., 2024b). To guarantee measurement reliability and assess data validity, each batch included three standard reference samples and one procedural blank, the latter showing values approximately 10^3 times lower than real samples. Results from repeated parallel tests (Fig. S3) indicated that uncertainties remained within the 2σ confidence interval.

https://doi.org/10.5194/egusphere-2026-3087
Preprint. Discussion started: 2 July 2026

2.5 Machine learning

Employing the XGBoost machine-learning model (Chen and Guestrin, 2016), we examined 20 years (2001–2020) of ERA5 reanalysis for the Tibetan Plateau region (25°N–40°N, 80°E–100°E), and used interpretable SHapley Additive exPlanations (SHAP) analysis to disentangle and quantify the influence of each meteorological parameter on rainfall (Lundberg et al., 2020) (Fig. S5). The predictors include: R1000 (relative humidity at 1000 hPa, %), CAPE (convective available potential energy, J/kg), Q1000 (specific humidity at 1000 hPa, g/kg), MSL (mean sea-level pressure, hPa), BLH (boundary-layer height, m), T2M (2-m air temperature, K), U50 (zonal wind at 50 hPa, m/s), Z200 (200-hPa geopotential height, m), U100 (100-m zonal wind, m/s), and V200 (100-m meridional wind, m/s). It should be noted that when applying SHAP analysis, the presence of interdependencies between features can lead to additive contribution effects, which may potentially affect the quantitative interpretation of the importance of individual features.

2.6 Trajectory calculations

The Hybrid Single-Particle Lagrangian Integrated Trajectory model (NOAA HYSPLIT. https://www.ready.noaa.gov/HYSPLIT.php) is a commonly used tool for tracking atmospheric transport and identifying air mass sources (Stein et al., 2015). To simulate the transport direction and speed of air masses at various altitudes, we employed 1°-resolution gridded meteorological data from the Global Data Assimilation System, with model settings consistent with those in prior research (Liu et al., 2024a). Air masses at different altitudes exhibit considerable differences in residence time and transport velocity. Accordingly, a trajectory duration of 72-96 hours was used in the simulations to adequately capture air mass movement. Three distinct inversion heights were

https://doi.org/10.5194/egusphere-2026-3087
Preprint. Discussion started: 2 July 2026

chosen to examine the vertical transport paths of the air masses. Due to the low and stable boundary layer in Xi'an, trajectory heights of 10 m, 500 m, and 1000 m above ground level were conventionally used. In comparison, Lhasa has more vigorous vertical air motions, with trajectory heights set at 10 m, 2000 m, and 6000 m above the ground to capture representative dynamics. Trajectory simulations began at periods of abnormal $^{10}Be/^{7}Be$ ratios, using a 6-hour interval for the initiation of each path. The model was initiated in December 2024, with backward trajectories traced from the two sampling locations (Lhasa: 29°38′49″N, 91°4′37″E; Xi'an: 34°13′20″N, 109°00′18″E).

2.7 Data collection and processing

The dataset, including Zonal (east-west) U wind speed and geopotential dataset, was obtained from ERA5 monthly averaged data on pressure levels (Hersbach et al., 2023) and visualized with Panoply. Origin 2020 was used to process and graph the raw data. Rainfall data were retrieved from the China Meteorological Data Network (http://data.cma.cn/). Annual fluxes of ^{7}Be and ^{10}Be were derived from mid-year average concentrations during the sampling period combined with annual precipitation data.

3. Results

^{7}Be and ^{10}Be wet deposition observations

Fig. 1a illustrates the time series of ^{10}Be and ^{7}Be concentrations and their daily deposition fluxes in Lhasa precipitation during the 2022–2023 rainy seasons (June to September). The concentrations of ^{10}Be and ^{7}Be varied from $(0.94 \pm 0.08)\cdot10^{4}$ atoms·g^{-1} to $(29.70 \pm 0.44)\cdot10^{4}$ atoms·g^{-1} rain, and from $(0.63 \pm 0.32)\cdot10^{4}$ atoms·g^{-1} rain to $(10.29 \pm 0.22)\cdot10^{4}$ atoms·g^{-1} rain,

https://doi.org/10.5194/egusphere-2026-3087
Preprint. Discussion started: 2 July 2026

respectively. Their median concentrations were $2.10 \cdot 10^4$ atoms·g^{-1} rain for ^{10}Be and $1.42 \cdot 10^4$ atoms·g^{-1} rain for ^{7}Be. The ^{10}Be/^{7}Be ratios varied between 0.97 ± 0.26 and 3.64 ± 0.32. The daily wet deposition fluxes of ^{10}Be and ^{7}Be in Lhasa, estimated using daily rainfall, ranged from (0.41 ± 0.02)$\cdot 10^8$ atoms·m^{-2}·d^{-1} to (43.07 ± 0.64)$\cdot 10^8$ atoms·m^{-2}·d^{-1} and from (0.29 ± 0.05)$\cdot 10^8$ atoms·m^{-2}·d^{-1} to (14.92 ± 0.31)$\cdot 10^8$ atoms·m^{-2}·d^{-1}, respectively. Median fluxes were $1.93 \cdot 10^8$ atoms·m^{-2}·d^{-1} for ^{10}Be and $0.98 \cdot 10^8$ atoms·m^{-2}·d^{-1} for ^{7}Be.

Fig. 1b illustrates the time series of ^{10}Be and ^{7}Be concentrations and daily wet deposition fluxes in precipitation in Xi'an during the same period (March to September 2023). In Xi'an, the concentration ranges of ^{10}Be and ^{7}Be in precipitation were (2.24 ± 0.10)$\cdot 10^4$ atoms·g^{-1} rain to (71.40 ± 0.63)$\cdot 10^4$ atoms·g^{-1} rain and (1.62 ± 0.22)$\cdot 10^4$ atoms·g^{-1} rain to (25.43 ± 0.79)$\cdot 10^4$ atoms·g^{-1} rain, respectively, with median values of $8.35 \cdot 10^4$ atoms·g^{-1} rain and $4.16 \cdot 10^4$ atoms·g^{-1} rain. The ^{10}Be/^{7}Be ratio ranged from 1.07 ± 0.09 to 2.81 ± 0.08. The daily wet deposition fluxes of ^{10}Be and ^{7}Be in Xi'an ranged from (1.28 ± 0.07)$\cdot 10^8$ atoms·m^{-2}·d^{-1} to (86.22 ± 1.83)$\cdot 10^8$ atoms·m^{-2}·d^{-1} and (0.68 ± 0.06)$\cdot 10^8$ atoms·m^{-2}·d^{-1} to (55.60 ± 3.08)$\cdot 10^8$ atoms·m^{-2}·d^{-1}, respectively, with median values of $8.32 \cdot 10^8$ atoms·m^{-2}·d^{-1} for ^{10}Be and $5.89 \cdot 10^8$ atoms·m^{-2}·d^{-1} for ^{7}Be. The specific measurements for each rainfall event are listed in Tables S1 and S2.

https://doi.org/10.5194/egusphere-2026-3087
Preprint. Discussion started: 2 July 2026

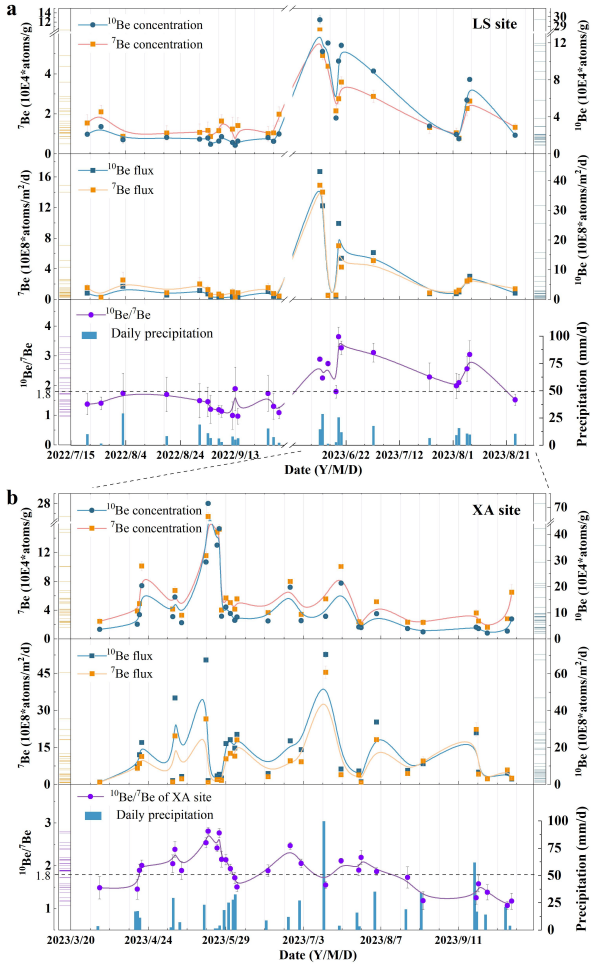

Fig. 1 Time series curves of wet settling of ^{10}Be and ^{7}Be. The concentrations, daily fluxes, and ratios of ^{10}Be and ^{7}Be in precipitation in the Lhasa, Tibetan Plateau (a) and the Xi'an, Loess Plateau (b). Xi'an's records only in 2023.

4. Discussion

4.1 Natural cosmogenic ^{10}Be and ^{7}Be fluxes

Cosmogenic ^{7}Be and ^{10}Be serve as robust tracers, enabling the quantification of Earth surface processes across timescales from daily to seasonal and on longer timescales of 10^3 to 10^5 years

https://doi.org/10.5194/egusphere-2026-3087
Preprint. Discussion started: 2 July 2026

(Brown et al., 1989; Graham et al., 2003; Juri Ayub et al., 2012; Deng et al., 2020). The key requirement for their application is a thorough understanding of the flux of ^{7}Be and ^{10}Be generated in the atmosphere and their transport to the Earth's surface. Around 95% of ^{10}Be and ^{7}Be in the atmosphere are deposited through wet deposition (Brown et al., 1989). Long-term, synchronized observational records of ^{10}Be and ^{7}Be in rainwater are limited, with the exception of our preliminary study in Xi'an, Loess Plateau (Zhang and Fu, 2017; Liu et al., 2024a). To the best of our knowledge, similar records exist only in regions such as the USA (Brown et al., 1989), New Zealand (Graham et al., 2003), and Switzerland (Heikkilä et al., 2008). This represents the first long-term daily-resolution observational record of atmospheric ^{10}Be and ^{7}Be wet deposition in the high-altitude regions of China, specifically the Tibetan Plateau (Fig. 1a). In light of the strong utility of ^{7}Be for investigating aerosol deposition, the joint use of ^{10}Be and ^{7}Be in our observations helps circumvent the natural-process constraints inherent to single-isotope tracers, paving the way for more precise quantitative assessments of bulk aerosol deposition rates.

The results reveal that the concentrations and ratios of ^{10}Be and ^{7}Be in precipitation from the Tibetan Plateau and Loess Plateau are broadly consistent with previous studies from other regions. Additionally, the ^{10}Be/^{7}Be ratio range in rainwater aligns with the dry deposition records of aerosols we previously collected from various locations across China (Liu et al., 2024b). According to the mean annual precipitation for the corresponding years in Lhasa (356.6 mm) and Xi'an (550.9 mm), the annual wet deposition fluxes of ^{10}Be and ^{7}Be in Lhasa (29°N) are $74.69 \cdot 10^{8}$ atoms$\cdot$m$^{-2}\cdot$yr^{-1} and $50.72 \cdot 10^{8}$ atoms$\cdot$m$^{-2}\cdot$yr^{-1}, respectively. In contrast, for Xi'an (34°N), the respective fluxes are $460.10 \cdot 10^{8}$ atoms$\cdot$m$^{-2}\cdot$yr^{-1} for ^{10}Be and $229.31 \cdot 10^{8}$ atoms$\cdot$m$^{-2}\cdot$yr^{-1} for ^{7}Be. The production rate ratio of ^{10}Be to ^{7}Be remains consistent across latitudes (Masarik et al., 1999).

https://doi.org/10.5194/egusphere-2026-3087
Preprint. Discussion started: 2 July 2026

Furthermore, our findings align with the modern trend of increasing ^{10}Be deposition flux with latitude, typically ranging from (40-530)·10^8 atoms·m^{-2}·yr^{-1} between latitudes 10° and 47° (Deng et al., 2020).

From these data, it can be seen that for Lhasa and Xi'an, which have similar annual mean precipitation, the ^{10}Be flux signal on an interannual scale mainly reflects changes in the production rate of ^{10}Be. This is consistent with previous studies, which concluded that on a seasonal scale, the flux variations of ^{7}Be and ^{10}Be are related to environmental factors such as precipitation rate and the height of the tropopause (Terzi and Kalinowski, 2017; Heikkilä and Smith, 2013). Therefore, the seasonal data of ^{10}Be and ^{7}Be may contain information on rainfall induced by monsoon circulation changes, particularly the daily resolution ^{10}Be and ^{7}Be flux data, which have the potential to record rapid rainfall variations.

4.2 ^{10}Be and ^{7}Be anomalies and rainfall changes

Owing to their high sensitivity to precipitation, ^{10}Be and ^{7}Be have become valuable tracers in environmental research. High rainfall events generally enhance the wet deposition fluxes of ^{10}Be and ^{7}Be, making them reliable proxies for reconstructing precipitation patterns. Leveraging this, ^{10}Be has been applied to paleo-precipitation reconstructions (Zhou et al., 2023), whereas ^{7}Be serves as a tracer for rainfall-induced soil erosion (Juri Ayub et al., 2012). In this study, we integrate precipitation-derived ^{10}Be and ^{7}Be records to assess how precipitation dynamics control beryllium deposition fluxes on daily to monthly timescales.

In Lhasa (two-year record) and Xi'an (one-year record), we fitted ^{10}Be and ^{7}Be concentrations and fluxes in precipitation against daily rainfall amounts (Fig. 2). The results reveal that ^{10}Be and ^{7}Be levels are closely tied to rainfall intensity (~0.5–100 mm·h^{-1}) during daily

https://doi.org/10.5194/egusphere-2026-3087
Preprint. Discussion started: 2 July 2026

precipitation events, suggesting a concurrent variation between rainfall intensity and the deposition behavior of beryllium isotopes. This phenomenon indicates that in modern environments, precipitation intensity will simultaneously regulate the deposition processes of both ^{7}Be and ^{10}Be.

Notably, the correlation between ^{10}Be and ^{7}Be fluxes and precipitation is substantially lower in Lhasa ($R^2 < 0.33$; Fig. 2c) than in Xi'an ($R^2 > 0.54$; Fig. 2d). This disparity may stem from the relatively sparse precipitation in Lhasa, where orographic uplift at high altitudes intensifies vertical atmospheric exchange, resulting in more pronounced interactions between precipitation dilution effects and dynamic atmospheric transport. In contrast, Xi'an experiences more abundant and concentrated rainfall events, contributing to the stronger flux-rainfall correlation observed. As highlighted by red-circled data in Fig. 2a and 2b, steeper slopes-indicative of elevated $^{10}Be/^{7}Be$ ratios: coincide with seasonal peaks in stratosphere-troposphere exchange. These elevated $^{10}Be/^{7}Be$ ratios reflect intensified stratosphere-troposphere exchange events (Zanis et al., 2003; Liu et al., 2024a). These findings imply that downward-transported stratospheric air masses, enriched in beryllium isotopes, intrude into the lower atmosphere and modulate rainfall and deposition patterns (Graham et al., 2003; Heikkilä et al., 2008). As a result, the additive signal during spring and summer appears subdued, likely because frequent convective rainfall events intensify dilution effects during deposition.

To isolate the contribution of stratosphere-to-troposphere vertical motion on ^{7}Be and ^{10}Be, we excluded data points with high $^{10}Be/^{7}Be$ ratios and conducted a re-analysis. This resulted in a significant improvement in the linear relationship between daily ^{7}Be and ^{10}Be wet deposition fluxes and rainfall amounts (Fig. 2c, 2d, $R^2 = 0.85\text{-}0.92$, $p < 0.05$) in both Lhasa and Xi'an. This

https://doi.org/10.5194/egusphere-2026-3087
Preprint. Discussion started: 2 July 2026

315 implies that, under regional tropospheric control, the deposition of ^{7}Be and ^{10}Be is predominantly
316 governed by precipitation. The slopes of these linear regression models provide a means to trace
317 environmental process variations over short-term (daily to seasonal) and long-term (10^{3}-10^{5} years)
318 timescales. This provides further insight into the mechanisms through which factors such as
319 precipitation, climate change, and stratosphere-troposphere exchange influence ^{7}Be and ^{10}Be
320 concentrations (Juri Ayub et al., 2012; Deng et al., 2020).
321

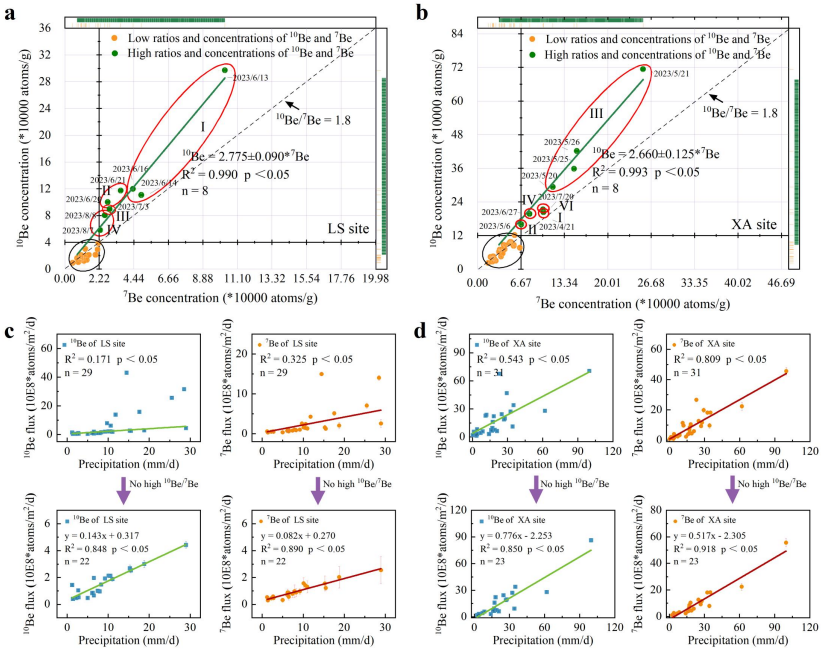

322

323 **Fig. 2** Linear fitting analysis of ^{10}Be, ^{7}Be, and daily precipitation. According to the observations
324 from Lhasa (a) and Xi'an (b), data points with ^{10}Be/^{7}Be ratios above the 1.8 baseline and relatively
325 high ^{10}Be and ^{7}Be concentrations are grouped into red circles based on their proximity in date and
326 labeled in chronological order, while the other points are grouped into a black circle. For the data
327 points in red circles (in Fig. 2a and 2b). Fig. 2c and 2d present linear fits of daily ^{10}Be and ^{7}Be

https://doi.org/10.5194/egusphere-2026-3087
Preprint. Discussion started: 2 July 2026

deposition fluxes versus daily precipitation, both before and after removing these points.

4.3 $^{10}Be/^{7}Be$ ratio traces atmospheric circulation changes

At the regional scale, precipitation is strongly modulated by atmospheric circulation patterns. Vertical atmospheric motions, especially under climate change, reinforce the established causal link between precipitation and circulation regimes. Cosmogenic ^{10}Be and ^{7}Be are recognized as sensitive tracers of atmospheric circulation dynamics (Raisbeck et al., 1981; Terzi and Kalinowski, 2017), with their distribution and deposition fluxes governed by circulation dynamics. Observational evidence (Fig. 1) shows elevated $^{10}Be/^{7}Be$ ratios in Lhasa and Xi'an, suggesting tropopause instability at the time, reflecting enhanced stratosphere-to-troposphere exchange, which elevated the relative input of ^{10}Be and consequently modified the $^{10}Be/^{7}Be$ ratio in precipitation.

Long-term (multiannual) trends of ^{7}Be are significantly influenced by solar activity and large-scale teleconnection indices, including the Arctic Oscillation (AO), North Atlantic Oscillation (NAO), and QBO (Chham et al., 2019). In contrast, ^{7}Be seasonal variations are mainly controlled by local meteorology (Chham et al., 2019; Abdul et al., 2025). Our sampling occurred during the rising phase of the 25th solar cycle (2019–2030), when solar activity is not a major driver of ^{7}Be or ^{10}Be trends (Gerasopoulos et al., 2003; Chham et al., 2019). QBO modulates the phase evolution of AO and NAO, with EQBO winters characterized by stronger stratosphere-troposphere coupling and amplified NAO patterns, whereas the opposite holds during WQBO years (Cai et al., 2022). Furthermore, multiyear records show that surface ^{7}Be levels oscillate in phase with QBO (Terzi and Kalinowski, 2017; Chham et al., 2019), with a significant

https://doi.org/10.5194/egusphere-2026-3087
Preprint. Discussion started: 2 July 2026

squared coherence (0.68, at the 90% confidence level) between the 20–30 month cycle of ^{7}Be and QBO (Gerasopoulos et al., 2003). The QBO descends at ~1 km/month, promoting stratosphere-to-troposphere exchange, thus elevating surface ^{7}Be levels. Meanwhile, ^{7}Be and ^{10}Be in precipitation show strong correlations in both flux and concentration ($R^2 \geq 0.92$, $P < 0.05$; Fig. S4), suggesting shared controls over their wet scavenging processes, and that they follow comparable temporal cycles. These synchronized shifts in ^{10}Be and ^{7}Be are tightly connected to QBO-driven changes in East Asian circulation, driving enhanced upper-atmosphere-to-surface cosmogenic beryllium transport. Therefore, during the active period of the summer monsoon, it is essential to closely monitor changes in the ^{10}Be/^{7}Be ratio to track vertical movements between the stratosphere and troposphere, which can trigger atmospheric circulation changes and lead to heavy rainfall.

4.4 Rainfall driving factors

Given that the independent indicators ^{10}Be and ^{7}Be in precipitation show that changes in atmospheric vertical structure have a significant impact on atmospheric circulation, we used long-term reanalysis data from the Tibetan Plateau (2021-2020) to train a machine learning XGBoost model. This model was used to analyze the contributions of various key precipitation driving factors and to clarify the driving process of atmospheric vertical motion on precipitation over the Tibetan Plateau under QBO modulation. Machine learning is adept at identifying nonlinear relationships between features, and here, interpretable machine learning is used to identify the key precipitation driving factors in precipitation activity over the Tibetan Plateau. The SHAP method was used to evaluate the output of the XGBoost model, quantifying the

https://doi.org/10.5194/egusphere-2026-3087
Preprint. Discussion started: 2 July 2026

372 contribution of individual variables to precipitation formation during the observed events, as
373 shown in Fig. 3a. The average absolute SHAP value across all samples represents the variable's
374 contribution to precipitation over the Tibetan Plateau region throughout the study period. The
375 positive or negative impact of this contribution is determined by the sign of the SHAP value (Fig.
376 3b).

377 The results show (Fig. 3), Tibetan Plateau precipitation is driven to different extents by a
378 range of meteorological variables: 1000 hPa relative humidity (R1000), convective available
379 potential energy (CAPE), 1000 hPa specific humidity (Q1000), mean sea-level pressure (MSL),
380 boundary-layer height (BLH), 2-m air temperature (T2M), zonal wind at 50 hPa (U50), 200 hPa
381 geopotential height (Z200), and 100-m zonal and meridional winds (U100, V100). The effects of
382 R1000 and Q1000 on total precipitation over the Tibetan Plateau are nonlinear (Fig. 3b), and
383 surpassing thresholds of 75% for R1000 and 10 g/kg for Q1000 markedly increases rainfall, with
384 the strongest positive impact located in the southern Plateau (Fig. 3c). Considering U100 and
385 V100, enhanced southeast winds primarily drive the increase in southern Tibetan Plateau rainfall,
386 while dominant westerlies inhibit precipitation (Fig. 3b). A similar pattern is observed in the
387 northern Plateau. Moisture influx from the Indian Ocean elevates relative humidity in the southern
388 Tibetan Plateau, thereby significantly promoting precipitation along the southern flank. In addition,
389 rising temperatures (T2M) intensify atmospheric convection, further augmenting rainfall.

390 It is noteworthy that in the EQBO phase (Fig. 3b, U50 negative), dominant upper-level
391 easterly winds markedly increase precipitation in the southern Tibetan Plateau. In contrast,
392 prevailing northwesterly westerlies at high altitudes during the WQBO phase inhibit rainfall
393 development. A similar pattern is observed in the northern Plateau. Convective available potential

https://doi.org/10.5194/egusphere-2026-3087
Preprint. Discussion started: 2 July 2026

394 energy (CAPE) and 200-hPa geopotential height (Z200) are tightly linked to atmospheric vertical
395 structure stability. Accordingly, the EQBO, by coupling and integrating upper-level vertical
396 circulation processes (CAPE and Z200, Fig. 3a), contributes as much as 31.3% to the Tibetan
397 Plateau's annual precipitation, primarily affecting the southern and central areas.

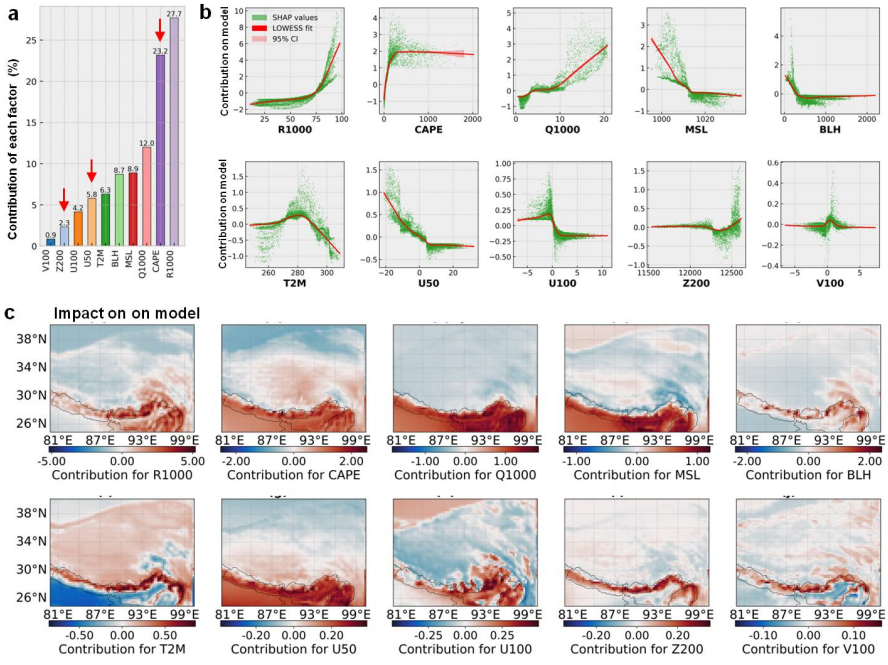

398

399 **Fig. 3** the principal factors controlling total rainfall over the Tibetan Plateau based on
400 machine-learning analysis. a. Using Shapley weighting analysis to explain the driving factors and
401 their contributions to total precipitation in the Tibetan Plateau from 2001 to 2020, as revealed by
402 the XGBoost machine learning model. b. Nonlinear dependence of SHAP values on total Tibetan
403 Plateau rainfall for different key predictors. SHAP dependence was visualized using Locally
404 Weighted Scatterplot Smoothing (LOWESS) (Cleveland. 1979) with a smoothing fraction of
405 frac=0.3 (using 30% of nearest neighbors for local regression) and it=3 robust iterations to reduce
406 outlier influence, and shaded band indicates 95% confidence interval (CI) of LOWESS regression.

https://doi.org/10.5194/egusphere-2026-3087
Preprint. Discussion started: 2 July 2026

c. Spatial patterns of SHAP values for key predictors and their contributions to total rainfall over the Tibetan Plateau. Analysis was conducted for 2001–2020. R1000: relative humidity at 1000 hPa (%), CAPE: convective available potential energy (J/kg), Q1000: specific humidity at 1000 hPa (g/kg), MSL: mean sea-level pressure (hPa); BLH: boundary layer height (m), T2M: 2 m air temperature (K); U50: zonal wind at 50 hPa (m/s), Z200: geopotential height at 200 hPa (m), U100: 100 m zonal wind (m/s), V200: 100 m meridional wind (m/s).

4.5 QBO-driven monsoon rainfall analysis

Reanalysis data for the 2022–2023 observation period (Fig. 4a) indicate that the upper-level zonal wind shifted from a westerly to an easterly phase, unlike the QBO disruption events during the 2015/16 and 2019/20 periods, which also featured zonal wind reversals, the QBO during 2022/23 underwent a stable and well-defined transition from WQBO to EQBO. The summer season is commonly when QBO wind direction transitions occur. During early summer (June), the geopotential height differences from 50 hPa to 850 hPa over East Asia generally shifted from negative to positive (Fig. 4b). In central and northern China, negative anomalies in geopotential height between 50 hPa and 200 hPa caused upper-level warm air to sink. During the EQBO phase, the subtropical high-pressure anomalies at 500 hPa and 850 hPa were more pronounced, strengthening the North Pacific High Center. Notably, the two high-pressure centers at approximately 850 hPa over the Tibetan Plateau and the Loess Plateau moved closer together, leading to abnormal near-surface uplift of air masses and increased moisture convergence in the region, thereby raising the probability of rainfall over these regions.

Currently, East Asian precipitation follows a dipole oscillation centered around 30°N latitude

https://doi.org/10.5194/egusphere-2026-3087
Preprint. Discussion started: 2 July 2026

(Zhang et al., 2024; Fu et al., 2024). The southern parts of the Tibetan Plateau and the Loess Plateau lie on the northern flank of the precipitation dipole, experiencing similar drought–flood regimes. In comparison to 2022, both the fluxes and the ratio of ^{10}Be to ^{7}Be in Lhasa showed a marked increase in 2023, suggesting that EQBO-related cyclonic activity favors the downward transport of background stratospheric easterly winds into the troposphere. Backward trajectory modeling further verifies that cyclonic anomalies during the ^{10}Be/^{7}Be enhancement periods reached the surface (Fig. 4c). Xi'an also experienced comparable increases in ^{10}Be and ^{7}Be in 2023, along with a corresponding downward transport process (Fig. 1b and 4d). These findings imply that such transport processes may have played a role in the ~60% rise in annual precipitation in Lhasa (from 273 mm in 2022 to 439 mm in 2023) and ~34% in Xi'an.

How does the QBO influence tropical summer zonal wind pathways to ultimately affect precipitation? Fig. 5a shows the composite differences in zonal wind across the pressure–latitude section averaged over 90–130°E during June–July between EQBO and WQBO years. We note that during the summer EQBO phase, the tropical stratosphere (30–60 hPa) exhibits easterly wind anomalies, accompanied by a prominent meridional–zonal wind dipole between the subtropics and high latitudes (e.g., easterly anomalies at 20–30°N and westerly anomalies at 30–40°N in June, shifting to 30–50°N and 50–75°N in July), which gradually shift northward over time, extending from the lower stratosphere to the lower troposphere. During this period, EQBO typically induces prevailing secondary anticyclonic circulations and sustains anomalous high-pressure systems (Hu et al., 2022). These secondary circulation cells may propagate downward, resulting in anomalous Rossby wave sources over East Asia, thereby triggering anomalous downward motion in the stratosphere, which strengthens the westerly jet stream and increases the ^{10}Be/^{7}Be ratio (Fig. 5b).

https://doi.org/10.5194/egusphere-2026-3087
Preprint. Discussion started: 2 July 2026

Meanwhile, the downward transport from the stratosphere can induce significant new formation of sulfate aerosols in the troposphere (Hugh Coe, 2024), which may be retained within the troposphere due to upward motions driven by the "suction pump" effect over the Tibetan Plateau, and radiate outward under the coupling effect of the westerly jet stream, ultimately interacting directly with radiation and acting as cloud condensation nuclei, potentially enhancing cloud and precipitation formation. Moreover, although sulfate variability has limited impact on global mean precipitation, it drives some of the most intense rapid precipitation responses over land (Richardson et al., 2018). Ultimately, vertical air mass motion, moisture flux, and thermal advection jointly drive the East Asian summer monsoonal precipitation anomalies.

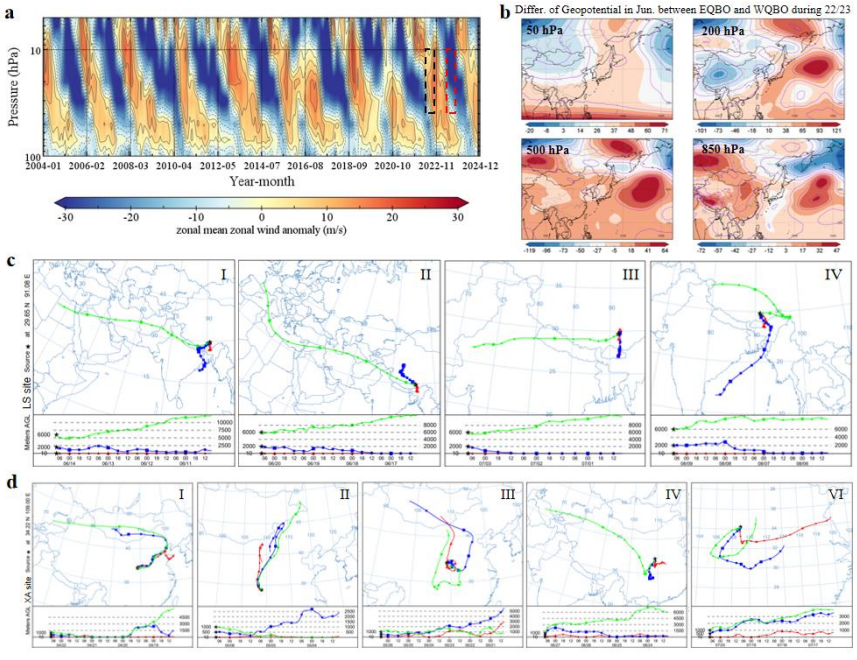

Fig. 4 Temporal-height evolution of zonal mean wind and geopotential, and backward trajectory simulation results. a. Time variation of the zonal mean zonal wind between 5°S and 5°N in 2004-2024, with black and red boxes representing WQBO in 2022 and EQBO in 2023,

https://doi.org/10.5194/egusphere-2026-3087
Preprint. Discussion started: 2 July 2026

464 respectively. The classification of QBO phases is based on the zonal mean wind around 30 hPa. b.
465 Differences in geopotential at 50 hPa, 200 hPa, 500 hPa, and 850 hPa between EQBO (2023) and
466 WQBO (2022) in June, derived by subtracting WQBO values from EQBO. The data are sourced
467 from the ERA5 reanalysis. c–d. Backward trajectory analysis results corresponding to periods of
468 anomalous $^{10}Be/^{7}Be$ ratios in Lhasa (c) and Xi'an (d). For Lhasa and Xi'an, four and five
469 simulations were conducted, respectively, and the numbering corresponds to those shown in Fig.
470 2a and 2b.

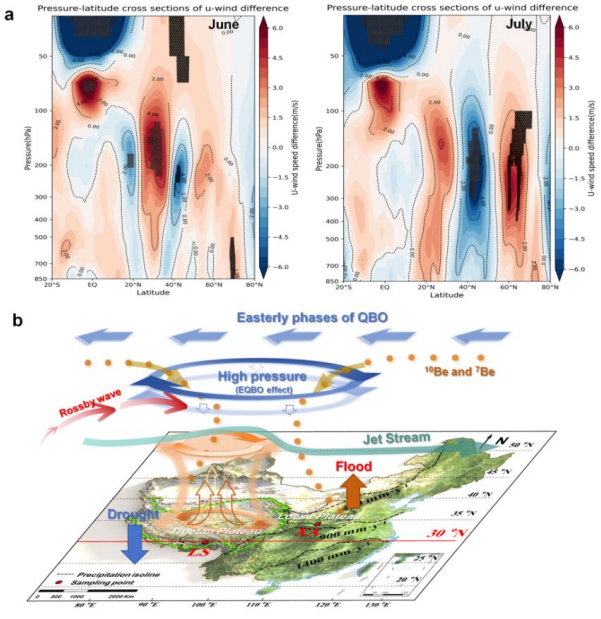

471

472 **Fig. 5** the schematic diagram of the combined difference between the easterly (EQBO) and
473 westerly (WQBO) phases and how EQBO modulates summer precipitation in East Asia. a.
474 Composite differences of the mean pressure latitude profile of zonal wind of 90°E-130°E in June
475 and July in the easterly phase (EQBO) and the westerly phase (WQBO) of the Quasi-Biennial
476 Oscillation years (2004-2023). The shaded area indicates significant anomalies between the two (p
477 < 0.05). b. Schematic diagram of ^{10}Be and ^{7}Be tracing EQBO modulation of East Asian summer

https://doi.org/10.5194/egusphere-2026-3087
Preprint. Discussion started: 2 July 2026

precipitation

5. Conclusion

The lack of understanding of the physical mechanisms linking stratospheric circulation and precipitation changes has limited current predictions of rainfall changes on the Qinghai Tibet Plateau. This work provides new facts and evidence, revealed directly by stratospheric tracers cosmogenic ^{7}Be and ^{10}Be, that precipitation over the southern Tibetan Plateau is influenced by the vertical structure changes of the stratospheric QBO during certain periods. The results showed that the median daily wet deposition fluxes of ^{10}Be and ^{7}Be in the southern Tibetan Plateau during the rainy season of 2022-2023 were $1.93 \cdot 10^{8}$ atoms$\cdot m^{-2} \cdot d^{-1}$ and $0.98 \cdot 10^{8}$ atoms$\cdot m^{-2} \cdot d^{-1}$, respectively, which were lower than the observation results of the adjacent Loess Plateau during the same period ($8.32 \cdot 10^{8}$ atoms$\cdot m^{-2} \cdot d^{-1}$ and $5.89 \cdot 10^{8}$ atoms$\cdot m^{-2} \cdot d^{-1}$, respectively), and the correlation with rainfall ($R^2<0.33$) was significantly lower than that in the Loess Plateau region ($R^2>0.54$). Among them, the invasion of ^{10}Be and ^{7}Be from the stratosphere troposphere is the main factor. Therefore, based on the $^{10}Be/^{7}Be$ ratio of stratospheric tracer, the dynamic effects of QBO modulation in the stratosphere were judged, and further machine learning XGBoost model was used to analyze that the coupling effect contributed up to 31.3%. Therefore, this is considered to provide a new perspective for the study of Asian summer rainfall mechanisms by utilizing stratospheric isotopic characteristics. Although the current study could not specifically determine the extent of circulation anomalies caused by the QBO based on the changes in ^{7}Be and ^{10}Be, this limitation does not detract from its validity as indirect evidence of this process. In future research, further characterizing the spatiotemporal variations of ^{7}Be and ^{10}Be fluxes at different altitudes and

https://doi.org/10.5194/egusphere-2026-3087
Preprint. Discussion started: 2 July 2026

latitudes, based on global ^{7}Be and ^{10}Be flux models, will help to address this shortcoming. Currently, the patterns of ^{7}Be and ^{10}Be fluxes and ratios can be used in practical applications to verify and supplement other established methods for studying global atmospheric phenomena, and may serve as an early warning indicator for QBO-modulated changes in the Asian summer monsoon circulation. In the future, we hope that this method can provide valuable information on atmospheric vertical transport for predicting extreme rainfall events caused by frequent deep convection in Asia.

Data availability

Rainfall data were retrieved from the China Meteorological Data Network (http://data.cma.cn/). The dataset, including Zonal (east-west) U wind speed and geopotential dataset, was obtained from ERA5 monthly averaged data on pressure levels (Hersbach et al., 2023). The ^{7}Be and ^{10}Be data from the southern Tibetan Plateau presented in the manuscript are available at https://www.lsdc.ac.cn/portal/data/2609.

Supplementary information

The Supporting Information is available free of charge.

Figures illustrating the sampling point locations, the experimental process of pre-processing experiments, and other experimental details and information of quality control experiments; tables illustrating the relevant content of sampling points ^{10}Be and ^{7}Be.

Competing interests

The authors state that they have no known competing financial interests or personal relationships that could affect the work described herein.

https://doi.org/10.5194/egusphere-2026-3087
Preprint. Discussion started: 2 July 2026

Author contributions

This manuscript was completed through the contributions of all authors. Xuke Liu and Yunchong Fu conceived the original idea, writing, visualization, and funding acquisition. Guocheng Dong, Li Zhang, and Xinyi Du have completed sampling, analysis, and review. Xuke Liu, Nanjian Liu, and Yanting Bi have completed the measurement and software. Yunchong Fu has completed the explanation and verification. Xuke Liu prepared the manuscript with the contributions of all co-authors.

Acknowledgments

This research has been supported by the National Natural Science Foundation of China (Grant No. 12575319, 12405336), the Innovation Capability Support Program of Shaanxi (Grant No. 2025RS-CXTD-036), the Youth Innovation Promotion Association CAS (Grant No. Y2021108), and the Natural Science Basic Research Program of Shaanxi (Grant No. 2024JC-YBQN-0298).

References

Abdul Rashid, F. I., Idris, M. I., Abdul Rahman, I., & Mohamed Zin, M. R. (2025). Meteorological effects on atmospheric radioactive particles: a review of recent research. Journal of Nuclear Science and Technology, 62(10), 881–914. https://doi.org/10.1080/00223131.2025.2519707

Baldwin, M. P., & Dunkerton, T. J. (1991). Quasi-Biennial Oscillation above 10 MB. Geophysical Research Letters, 18(7), 1205–1208. doi:10.1029/91gl01333

Bian, J., Li, D., Bai, Z., Li, Q., Lyu, D., & Zhou, X. (2020). Transport of Asian surface pollutants to the global stratosphere from the Tibetan Plateau region during the Asian summer monsoon.

https://doi.org/10.5194/egusphere-2026-3087
Preprint. Discussion started: 2 July 2026

National Science Review. doi:10.1093/nsr/nwaa005

Brown, L., Stensland, G. J., Klein, J., & Middleton, R. (1989). Atmospheric deposition of 7Be and 10Be. Geochimica et Cosmochimica Acta, 53(1), 135-142. doi:10.1016/0016-7037(89)90280-9

Cai, Q., Chen, W., Chen, S., Ma, T., & Garfinkel, C. I. (2022). Influence of the Quasi-Biennial Oscillation on the spatial structure of the wintertime Arctic oscillation. Journal of Geophysical Research: Atmospheres, 127, e2021JD035564. doi: 10.1029/2021JD035564

Chen Peng, Yi Peng, Czymzik Markus, et al. (2020). Relationship between precipitation and 10Be and impacts on soil dynamics. Catena, 195, 104748. doi: org/10.1016/j.catena.2020.10474

Chham, E., Milena-Pérez, A., Piñero-García, F., Hernández-Ceballos, M. A., Orza, J. A. G., Brattich, E., … Ferro-García, M. A. (2019). Sources of the seasonal-trend behaviour and periodicity modulation of 7Be air concentration in the atmospheric surface layer observed in southeastern Spain. Atmospheric Environment, 213, 148-158. doi:10.1016/j.atmosenv.2019.06.011

Chen T., Guestrin C., XGBoost: a scalable tree boosting system. In Proceedings of the 22nd ACM SIGKDD International Conference on Knowledge Discovery and Data Mining, San Francisco, California, USA. 785-794 (2016). doi: 10.1145/2939672.2939785

Collimore, C. C., Martin, D. W., Hitchman, M. H., Huesmann, A., & Waliser, D. E. (2003). On The Relationship between the QBO and Tropical Deep Convection. Journal of Climate, 16(15), 2552–2568. doi:10.1175/1520-0442(2003)016<2552:otrbtq>2.0.co;2

Cleveland W. S. Robust Locally Weighted Regression and Smoothing Scatterplots. Journal of the American Statistical Association. 1979. 74(368), 829-836. doi: 10.2307/2286407

https://doi.org/10.5194/egusphere-2026-3087
Preprint. Discussion started: 2 July 2026

566 Deng, K., Wittmann, H., & von Blanckenburg, F. (2020). The depositional flux of meteoric
567 cosmogenic 10Be from modeling and observation. Earth and Planetary Science Letters, 550,
568 116530. doi:10.1016/j.epsl.2020.116530
569 Ebdon, R. A., & Veryard, R. G. (1961). Fluctuations in equatorial stratospheric winds. Nature,
570 189(4767), 791-793. doi: org/10.1038/189791a0
571 Fu Z H, Zhou W, Xie S P, Zhang R, Wang X. 2024. Dynamic pathway linking Pakistan flooding to
572 East Asian heatwaves. Sci Adv, 10: eadk9250. doi: 10.1126/sciadv.adk9250
573 Gerasopoulos, E., Zerefos, C. ., Papastefanou, C., Zanis, P., & O' Brien, K. (2003). Low-frequency
574 variability of beryllium-7 surface concentrations over the Eastern Mediterranean.
575 Atmospheric Environment, 37(13), 1745-1756. doi:10.1016/s1352-2310(03)00068-2
576 Graham, I., Ditchburn, R., & Barry, B. (2003). Atmospheric deposition of 7Be and 10Be in New
577 Zealand rain (1996-98). Geochimica et Cosmochimica Acta, 67(3), 361-373.
578 doi:10.1016/s0016-7037(02)01092-x
579 Heikkilä, U., & Smith, A. M. (2013). Production rate and climate influences on the variability of
580 10Be deposition simulated by ECHAM5-HAM: Globally, in Greenland, and in Antarctica.
581 Journal of Geophysical Research: Atmospheres, 118(6), 2506-2520. doi:10.1002/jgrd.50217
582 Heikkilä, U., Beer, J., & Alfimov, V. (2008). Beryllium-10 and beryllium-7 in precipitation in
583 Dübendorf (440 m) and at Jungfraujoch (3580 m), Switzerland (1998–2005). Journal of
584 Geophysical Research, 113(D11). doi:10.1029/2007jd009160
585 Hersbach, H., Bell, B., Berrisford, P., Biavati, G., Horányi, A., Muñoz Sabater, J., Nicolas, J.,
586 Peubey, C., Radu, R., Rozum, I., Schepers, D., Simmons, A., Soci, C., Dee, D., Thépaut, J-N.
587 (2023): ERA5 monthly averaged data on pressure levels from 1940 to present. Copernicus

https://doi.org/10.5194/egusphere-2026-3087
Preprint. Discussion started: 2 July 2026

588 Climate Change Service (C3S) Climate Data Store (CDS), doi:10.24381/cds.6860a573,
589 *Accessed on <8 December, 2024>*.
590 Hitchman, M. H., Yoden, S., Haynes, P. H., Kumar, V., & Tegtmeier, S. (2021). An observational
591 history of the direct influence of the stratospheric quasi-biennial oscillation on the tropical
592 and subtropical upper troposphere and lower stratosphere. Journal of the Meteorological
593 Society of Japan, 99(2), 239–267. doi: 10.2151/jmsj.2021-012
594 Ho, C. H., Kim, H. S., Jeong, J. H., & Son, S. W. (2009). Influence of stratospheric quasi-biennial
595 oscillation on tropical cyclone tracks in the western North Pacific. Geophysical Research
596 Letters, 36(6), L06702.doi: 10.1029/2009GL03716
597 Hu Jinggao, Gao Xiang, Ren Rongcai, et al. 2022. On the relationship between the stratospheric
598 quasi-biennial oscillation and summer precipitation in northern China. Geophysical Research
599 Letters, 49, e2021GL097687.doi: 10.1029/2021GL097687
600 Hugh Coe, Particle resupply in the lower atmosphere. Science 385, 144-144(2024). doi:
601 10.1126/science.adq4711
602 IPCC. 2021. Climate Change 2021: The Physical Science Basis. Cambridge: Cambridge
603 University Press
604 Juri Ayub, J., Lohaiza, F., Velasco, H., Rizzotto, M., Di Gregorio, D., & Huck, H. (2012).
605 Assessment of 7Be content in precipitation in a South American semi-arid environment.
606 Science of The Total Environment, 441, 111–116. doi: 10.1016/j.scitotenv.2012.09.079
607 Li Y, Zhao S and Wang G (2021) Spatiotemporal Variations in Meteorological Disasters and
608 Vulnerability in China During 2001-2020. Front. Earth Sci. 9:789523. doi:
609 10.3389/feart.2021.789523

https://doi.org/10.5194/egusphere-2026-3087
Preprint. Discussion started: 2 July 2026

610 Liu XK, Fu YC, Bi YT, Zhang L, Zhao GQ, Xian F, et al. Monitoring Surface Be-10/Be-7 Directly
611 Reveals Stratospheric Air Intrusion in Sichuan Basin, China. Journal Of Geophysical
612 Research-Atmospheres 2022; 127. doi: 10.1029/2022JD036543
613 Liu, XK., Fu, YC., Zhang, L. et al. Cosmogenic radionuclide Beryllium-7 and Beryllium-10
614 characteristics and influencing factors in different natural climate regions, China, Science of
615 the Total Environment, 2024b, 945:174146 doi: 10.1016/j.scitotenv.2024.174146
616 Liu, XK, Fu, YC, Zhang, L. et al. Deep stratospheric intrusion events in China revealed on the
617 ground by cosmogenic 10Be/7Be. Commun Earth Environ 5, 553 (2024a). doi:
618 10.1038/s43247-024-01727-7
619 Luo, F., Luo, J., Xie, F., et al. The Key Role of the Vertical Structure of the Stratospheric
620 Quasi-Biennial Oscillation in the Variations of Asian Precipitation in Summer. Geophysical
621 Research Letters, 2023, 50(24): e2023GL105863.
622 Lundberg, S. M., Erion, G. , Chen, H. , et al. From local explanations to global understanding with
623 explainable AI for trees. Nat. Mach. Intell. 2, 56-67 (2020). doi: 10.1038/s42256-019-0138-9
624 Masarik, J., & Beer, J. (1999). Simulation of particle fluxes and cosmogenic nuclide production in
625 the Earth's atmosphere. Journal of Geophysical Research: Atmospheres, 104(D10),
626 12099–12111. doi: 10.1029/1998jd200091
627 MA Yaoming , MA Weiqiang , DAI Huaguang, et al. 2023, Earth summit mission 2022: Scientific
628 expedition and research on Mt.Qomolangma helps reveal the synergy between westerly
629 winds and monsoon and the resulting climatic and environmentaleffects. Adv. Atmos. Sci.,
630 40(2), 187−193, https://doi.org/10.1007/s00376-022-2166-3.
631 Raisbeck, G. M., Yiou, F., Fruneau, M., Loiseaux, J. M., Lieuvin, M., & Ravel, J. C. (1981).

https://doi.org/10.5194/egusphere-2026-3087
Preprint. Discussion started: 2 July 2026

632 Cosmogenic 10Be/7Be as a probe of atmospheric transport processes. Geophysical Research
633 Letters, 8(9), 1015–1018. doi: 10.1029/gl008i009p01015
634 Richardson, T. B., and Coauthors, 2018: Drivers of Precipitation Change: An Energetic
635 Understanding. J. Climate, 31, 9641–9657, doi: 10.1175/JCLI-D-17-0240.1.
636 Stein, A. F., Draxler, R. R., Rolph, G. D., Stunder, B. J. B., Cohen, M. D., & Ngan, F. (2015).
637 NOAA's HYSPLIT Atmospheric Transport and Dispersion Modeling System. Bulletin of the
638 American Meteorological Society, 96(12), 2059–2077. doi: 10.1175/bams-d-14-00110.1
639 Terzi, L., & Kalinowski, M. (2017). World-wide seasonal variation of 7Be related to large-scale
640 atmospheric circulation dynamics. Journal of Environmental Radioactivity, 178-179, 1–15.
641 doi: 10.1016/j.jenvrad.2017.06.031
642 Tiessen, C., Bemmerer, D., Rugel, G. et al. Accelerator mass spectrometry (AMS) for beryllium-7
643 measurements in smallest rainwater samples. J Radioanal Nucl Chem 319, 965–973 (2019).
644 doi: 10.1007/s10967-018-6371-6
645 Willner, S.N., Otto, C. & Levermann, A. Global economic response to river floods. Nature Clim
646 Change 8, 594-598 (2018). doi: 10.1038/s41558-018-0173-2
647 Yamagata, T., Sugihara, S., Morinaga, I., Matsuzaki, H., & Nagai, H. (2010). Short term variations
648 of 7Be, 10Be concentrations in atmospheric boundary layer. Nuclear Instruments and
649 Methods in Physics Research Section B: Beam Interactions with Materials and Atoms,
650 268(7-8), 1135–1138. doi:10.1016/j.nimb.2009.10.117
651 Yang, K., Wu, H., Qin, J., Lin, C., Tang, W., & Chen, Y. (2014). Recent climate changes over the
652 Tibetan Plateau and their impacts on energy and water cycle: A review. Global and Planetary
653 Change, 112, 79–91. doi: 10.1016/j.gloplacha.2013.12.001

https://doi.org/10.5194/egusphere-2026-3087
Preprint. Discussion started: 2 July 2026

654 Yu Haoran, Lin Yuchi, Cao Fang, et al., (2025). Isotopic Observations Reveal Divergent Origins
655 and Formation Pathways of Atmospheric Nitrate in Aerosols and Rainwater, Environmental
656 Science & Technology, 59(45). doi:10.1021/acs.est.5c13801
657 Zanis, P. (2003). An estimate of the impact of stratosphere-to-troposphere transport (STT) on the
658 lower free tropospheric ozone over the Alps using10Be and7Be measurements. Journal of
659 Geophysical Research, 108(D12). doi: 10.1029/2002jd002604
660 Zhang, L., & Fu, Y.-C. (2017). Preliminary study of 10Be/7Be in rainwater from Xi'an by
661 Accelerator Mass Spectrometry. Chinese Physics C, 41(1), 018201. doi:
662 10.1088/1674-1137/41/1/018201
663 Zhang R, Zhou W, Tian W, Zhang Y, Zhang J, Luo J. 2024. A stratospheric precursor of East Asian
664 summer droughts and floods. Nat Commun, 15: 247. doi: 10.1038/s41467-023-44445-y
665 Zhang R, Zhou W. 2023. Decadal change in the linkage between QBO and the leading mode of
666 Southeast China winter precipitation. J Clim, 36: 7379–7392. doi:
667 10.1175/JCLI-D-23-0028.1
668 Zhou, Weijian., Kong, Xianghui., Paterson, Greig A., et al., Eccentricity-paced geomagnetic field
669 and monsoon rainfall variations over the last 870 kyr. Proc. Natl. Acad. Sci. 120,
670 e2211495120 (2023). doi: 10.1073/pnas.2211495120